



Environmental
Science
Nano

**Nanoparticle size and natural organic matter composition
determine aggregation behavior of polyvinylpyrrolidone
coated platinum nanoparticles**

Journal:	<i>Environmental Science: Nano</i>
Manuscript ID	EN-ART-06-2020-000659.R2
Article Type:	Paper

SCHOLARONE™
Manuscripts

Environmental significance

This study provides insights on the aggregation of polyvinylpyrrolidone coated platinum nanoparticle (PVP-PtNP) based on PVP-PtNP primary particle size and the molecular properties of natural organic matter (NOM). The aggregate size of PtNP increased with decreasing primary PVP-PtNP size. 20 nm PVP-PtNP (PVP-PtNP₂₀) formed aggregates in the presence and absence of the same NOM samples, and aggregate size increased in the presence of NOM. The aggregate size of PVP-PtNP₂₀ (1) increased with increasing NOM elemental ratio of H to C and the relative abundance of lignin-like compounds/carboxyl rich alicyclic molecules, and (2) decreased with increasing NOM molecular weight, SUVA₂₅₄, elemental ratio of O to C, and the relative abundance of condensed hydrocarbons-, and tannin – like compounds. These results reveal that the molecular properties of NOM, and thus composition and sources, are key factors that contribute to the stability of PtNPs in the aquatic environment.

1
2
3 **Nanoparticle size and natural organic matter composition determine**
4 **aggregation behavior of polyvinylpyrrolidone coated platinum**
5 **nanoparticles**
6
7
8
9

10
11 Mithun Sikder¹, Jingjing Wang¹, Brett A. Poulin^{2,3}, Malak M. Tfaily^{4,5}, Mohammed
12 Baalousha^{1,*}
13

14
15
16 ¹ *South Carolina SmartState Center for Environmental Nanoscience and Risk (CENR),*
17 *Department of Environmental Health Sciences, University of South Carolina, Columbia,*
18 *SC, 29208, United States*
19

20
21
22 ² *U.S. Geological Survey, Boulder, CO, 80303, United States*
23

24
25 ³ *Department of Environmental Toxicology, University of California Davis, Davis, CA*
26 *95616, United States*
27

28
29 ⁴ *Environmental Molecular Sciences Laboratory, Richland, WA 99354, United States*
30

31
32 ⁵ *Department of Environmental Science, University of Arizona, AZ 85721, United States*
33
34
35
36

37 **Correspondence:** Dr. Mohammed Baalousha, Department of Environmental Health
38 Sciences, University of South Carolina, 921 Assembly Street, Columbia, SC, 29208,
39 USA, Tel: +1 803-777-7177, E-mail: mbaalous@mailbox.sc.edu
40
41
42
43
44
45
46
47
48
49
50
51
52
53
54
55
56
57
58
59
60

Abstract

Engineered nanoparticle (NP) size and natural organic matter (NOM) composition play important roles in determining NP environmental behaviors. The aim of this work was to investigate how NP size and NOM composition influence the colloidal stability of polyvinylpyrrolidone coated platinum engineered nanoparticles (PVP-PtNPs). We evaluated PVP-PtNP aggregation as a function of the NP size (20, 30, 50, 75, and 95 nm, denoted as PVP-PtNP₂₀₋₉₅) in moderately hard water (MHW). Further, we quantified the effect of the hydrophobic organic acid (HPOA) fraction of NOM on the aggregation of PVP-PtNP₂₀ and PVP-PtNP₉₅ using 6 NOM samples from various surface waters, representing a range of NOM compositions and properties. NOM samples were characterized for bulk elemental composition (*e.g.*, C, O, N, and S), specific ultraviolet absorbance at 254 nm (SUVA₂₅₄), and molecular level composition (*e.g.*, compound classes) using ultrahigh resolution mass spectrometry. Single particle-inductively coupled plasma-mass spectrometry (sp-ICP-MS) was employed to monitor the aggregation of PVP-PtNPs at 1 μg PVP-PtNP L⁻¹ and 1 mg NOM L⁻¹ concentrations. PVP-PtNP aggregate size increased with decreasing primary PVP-PtNP size, likely due to the lower zeta potential, the higher number concentration, and the higher specific surface area of smaller NPs compared to larger NPs at the same mass concentration. No aggregation was observed for PVP-PtNP₉₅ in MHW in presence and absence of the different NOM samples. PVP-PtNP₂₀ formed aggregates in MHW in the presence and absence of the six NOM samples, and aggregate size increased in the presence of NOM likely due to interparticle bridging of NOM-coated PVP-PtNPs by divalent counterions. PVP-PtNP₂₀ aggregate size increased with the increase in NOM elemental ratio of H to C and the relative abundance of lignin-like/carboxyl rich-alicyclic molecules (CRAM)-like compounds. However, the aggregate size of PVP-PtNP₂₀ decreased with the increase in NOM molecular weight, NOM SUVA₂₅₄, elemental ratio of O to C, and the relative abundance of condensed hydrocarbons-, and tannin-like compounds. Overall, the results of this study suggest that the composition and sources of NOM are key factors that contribute to the stability of PVP-PtNPs in the aquatic environment.

INTRODUCTION

The colloidal stability of engineered nanoparticles (NPs) has been studied extensively over the past two decades. Numerous studies measured NP aggregation for different types of NPs with a major focus on investigating the effect of NP surface coating, media ionic strength, ion valency, and natural organic matter (NOM)^{1, 2}. Yet, there is a limited and often contradictory knowledge on the effect of both NP size and NOM properties on the aggregation of NPs. For instance, whereas some studies reported a decrease in the critical coagulation concentration (CCC, the minimum counterion concentration required to fully destabilize the dispersion) with the decrease in NP size (*e.g.*, hematite³, TiO₂⁴), others reported an increase in CCC with the increase in NP size (*e.g.*, CdSe NP⁵), or an independence of CCC and NP size (*e.g.*, AuNPs⁶, AgNPs², PtNPs⁷). Further, some studies reported a positive linear correlation between the CCC and NP size (*e.g.*, anatase TiO₂⁴), while others found that the CCC correlated better with NP specific surface area (*e.g.*, TiO₂⁴, CdSe NP⁵), and another study reported no correlation between CCC and NP size and/or specific surface area in the presence of monovalent and divalent electrolytes (*e.g.*, PtNPs⁷).

NOM is ubiquitous in the environment with concentrations in major rivers commonly between 1 to 10 mg-C L⁻¹, depending on biochemical and climatic conditions⁸⁻¹⁰. NOM is a complex mixture of polyelectrolytic and polyfunctional organic molecules (*e.g.*, polysaccharides, proteins, lipids, nucleic acids, and fulvic and humic substances)¹¹,¹² that vary spatially and temporally in terms of molecular composition, acidity, molecular weight, structure, and charge density¹³. The adsorption of NOM on NP surfaces¹⁴ results in the formation of an NOM-corona¹⁵, giving NPs a unique surface identity, which may determine the environmental behavior of NPs. NOM can act as a competitor to displace intentional engineered coatings (*e.g.*, citrate, polyvinylpyrrolidone, PVP) on NPs. For instance, NOM molecules (*i.e.*, both humic and fulvic acids) can displace citrate coatings from the surfaces of AgNPs¹⁶ and AuNPs¹⁷ due to the higher affinity of NOM molecules for NP surfaces. Model thiol ligands (*e.g.*, cysteine) can replace the PVP coating on AgNPs¹⁸, which suggests that thiol groups present in NOM may play an important role in determining NOM interfacial interactions with PVP-coated NPs. NOM can enhance NP stability by enhancing NP electrostatic repulsion and/or steric hindrance¹⁹⁻²¹. However, the impact of NOM on the environmental behaviors of NPs depends on the properties of NOM such as charge density, functional groups, and molecular weight²².

1
2
3 For instance, higher molecular weight NOM increases the stability of AuNPs due to
4 increased electrosteric repulsion²²⁻²⁵. The aggregation of ZnS NPs decreased with
5 increasing NOM concentration, the molecular weight and aromatic content of NOM
6 fractions, while the carboxylate and reduced sulfur content of NOM had little effect²⁶.

7
8
9
10 Recently, the application of ultrahigh resolution mass spectrometry, specifically
11 Fourier transform-ion cyclotron resonance-mass spectroscopy (FT-ICR-MS), to natural
12 matrices has offers resolving power sufficient to identify the molecular formulas of
13 thousands of unique molecules that make up NOM. FT-ICR-MS measures the mass-to-
14 charge ratio of organic molecules with up to six decimal place precision²⁷, and allows
15 the discrimination of compositional differences between different NOM samples.
16 Similarly, recent developments in single particle inductively coupled plasma mass
17 spectrometry (sp-ICP-MS) allows measuring NP size and aggregation at environmentally
18 relevant NP concentrations²⁸. Such measurements and understanding have been limited
19 by the detection limits of commonly implemented analytical techniques for NP sizing and
20 aggregation such as dynamic light scattering (DLS) and nanoparticle tracking analysis
21 (NTA). These methods require high NP concentrations, typically in the mg L⁻¹ range²⁹,
22 which is well above the predicted environmental concentrations of most NPs (*e.g.*, ng L⁻¹
23 to µg L⁻¹)^{30,31}. At such high concentrations, NPs aggregate at faster rates, form larger
24 aggregates, are more likely to settle out of solution, and dissolve at slower rates³².
25 Together, data obtained by FT-ICR-MS on NOM molecular composition and by sp-ICP-
26 MS on NP aggregation, will advance the understanding of the changes in NP aggregation
27 that are associated with changing NOM conditions (*e.g.*, concentrations and molecular
28 composition) under environmentally relevant low NP concentrations.

29
30
31
32
33
34
35
36
37
38
39
40
41
42
43 The release of platinum into the environment has increased due to widespread use
44 in automobile catalysts³³⁻³⁸ and some studies demonstrated that the release of Pt in road
45 dust is in the form of nanoparticles³⁹. The expected Pt concentration is 0.4-10.8 ng L⁻¹ in
46 aquatic ecosystems and 50 ng kg⁻¹ in the road dust⁴⁰. The occurrence of PtNPs in the
47 environment raises concerns regarding the potential environmental implications (*e.g.*,
48 bioaccumulation and/or toxicity) of PtNPs⁴¹. Several studies reported bioaccumulation
49 and toxicological effects of Pt in aquatic organisms, such as water fleas⁴², freshwater
50 oligochates⁴³, microalgae⁴⁴, and marine bacteria⁴⁵.

51
52
53
54
55
56
57
58
59
60
The aims of this study were to determine the impacts of 1) the primary particle
size of NPs, and; 2) the properties and the molecular composition of the hydrophobic

1
2
3 organic acid (HPOA) fraction of NOM on the aggregation behavior of PVP-PtNPs at
4 environmental relevant NP concentrations using state-of-the-art analytical techniques of
5 sp-ICP-MS and FT-ICR-MS.
6
7
8
9

10 **METHODOLOGY**

11 *NP synthesis*

12
13 Polyvinylpyrrolidone coated platinum engineered nanoparticles (PVP-PtNPs)
14 were synthesized according to the approach described by Sikder et al (2018) ⁷. First,
15 citrate coated platinum engineered nanoparticles (cit-PtNPs) of different sizes (*e.g.*, 10,
16 17, 31.6, 59.3, 53.5 nm, measured by DLS) were synthesized using seed-mediated growth
17 approach as described elsewhere ⁷. Second, PVP-PtNPs (PtNP₂₀, PtNP₃₀, PtNP₅₀, PtNP₇₅,
18 PtNP₉₅) were obtained by a ligand exchange approach using cit-PtNPs as precursors.
19 Briefly, 300 mL cit-PtNPs of different sizes (*e.g.*, 10, 17, 31.6, 59.3, 53.5 nm) were
20 converted into PVP-PtNPs by adding 1.0, 0.85, 0.48, 0.20, and 0.12 mL of 7.7 mM PVP
21 solution, respectively, under vigorous stirring (700 rpm) for at least 1 h. The PVP amount
22 selected was that required to obtain a surface coverage of 8 PVP molecules nm⁻²
23 according to the method presented elsewhere ⁷. PVP coating was used to obtain to obtain
24 stable engineered nanoparticles with uniform size distributions ⁴⁶. Additionally, PVP
25 coating was used as a model coating because it is one of the widely used capping agent
26 in the synthesis of engineered nanoparticles allowing comparison to other studies.
27
28
29
30
31
32
33
34
35
36
37
38
39
40

41 *Nanoparticle characterizations*

42
43 The core size and morphology of the synthesized PVP-PtNPs (PtNP₂₀-PtNP₉₅)
44 were measured using transmission electron microscopy (TEM, LaB₆ Jeol 2100, 200 KeV,
45 MA, USA). Samples for TEM analysis were prepared by depositing a droplet of undiluted
46 PVP-PtNP suspension on a 300-mesh carbon coated Cu-grid (Agar Scientific, Stansted,
47 UK) for 15 mins followed by rinsing with ultra-pure water (UPW). The grids were then
48 left to dry at room temperature for 48 h in a covered petri dish. The elemental composition
49 of the synthesized PVP-PtNPs was confirmed by Energy Dispersive X-ray Spectroscopy
50 (EDS, Jeol EX-230 Silicon Drift Detector, MA, USA) coupled with the TEM. Particle
51 size was measured using the Gatan Digital Micrograph software package (GMS 3) ⁴⁷. At
52 least 150 individual NPs were analyzed to determine the particle size distribution (PSD)
53
54
55
56
57
58
59
60

1
2
3 and the mean size. The z-average hydrodynamic diameter (Z_{avg}), polydispersity index
4 (PDI), and electrophoretic mobility of the synthesized PVP-PtNPs were determined by
5 dynamic light scattering (DLS) and laser Doppler electrophoresis using a Zetasizer Nano-
6 ZS instrument (Malvern Instruments Ltd., MA, USA). The Z_{avg} and zeta potential were
7 determined only at high particle concentrations ($> 1 \text{ mg L}^{-1}$), where robust zeta potential
8 measurements were obtained. The theoretical particle number concentration of $1 \mu\text{g L}^{-1}$
9 PVP-PtNPs was calculated by dividing the mass concentration by the average primary
10 particle mass, which was calculated using particle density (21.45 g cm^{-3}) and diameter as
11 measured by TEM.
12
13
14
15
16
17
18
19

20 *NOM Samples*

21
22 The HPOA fraction of NOM was isolated from a wide range of aquatic
23 environments (details in **Table S1**) including: three saw-grass dominated wetlands in the
24 northern Florida Everglades Water Conservation Area (WCA) 2A at site F1 (NOM 1),
25 WCA 2B South (NOM 2), and Arthur R. Marshall Loxahatchee National Wildlife Refuge
26 (LOX) at site 8 (NOM 6); the Suwannee River (Georgia; NOM 5), Williams lake
27 (Minnesota; NOM 3); and Pacific Ocean surface water near Hawaii (NOM 4). The HPOA
28 fraction of NOM was isolated on XAD-8 resin⁴⁸, which is a chemically distinct NOM
29 fraction that is recognized as reactive to natural⁴⁹ and engineered NPs⁵⁰ and is a suitable
30 fraction of NOM to represent the most influential NOM molecules in natural waters. NOM
31 samples were freeze-dried immediately after isolation to minimize NOM alteration prior
32 to NP stability experiments. Additional details on the isolation of the Everglades⁵¹ and
33 Pacific Ocean samples⁵² are available elsewhere. Solid-phase extraction is obligatory for
34 the NOM analyses made in this study and experiments with NPs. Specifically, the solid-
35 phase extraction produces a salt-free extract that is necessary for FTICR-MS analysis.
36 Further, the use of salt-free NOM samples in NP stability experiments allows experiments
37 to be performed under the identical aqueous conditions (*i.e.*, not influenced by inorganic
38 ions from the different NOM samples). Isolation of NOM by solid-phase extraction on
39 XAD resins and use of alkaline solution is the method recommended by the International
40 Humic Substances Society. Properties of NOM samples including the bulk elemental
41 compositions and specific ultraviolet absorbance at 254 nm (SUVA_{254}) are provided in
42 **Table S1**^{53, 54}.
43
44
45
46
47
48
49
50
51
52
53
54
55
56
57
58
59
60

Molecular characterization of NOM using FT-ICR-MS

NOM samples were reconstituted directly in HPLC-grade methanol at a concentration of 20 mg L⁻¹ and analyzed by FT-ICR-MS by direct injection in negative ionization mode. A 12 Tesla Bruker Solarix FT-ICR-MS located at the Environmental Molecular Sciences Laboratory in Richland, WA, was used to collect ultrahigh-resolution mass spectra of the NOM samples. A standard Bruker electrospray ionization (ESI) source was used to generate negatively charged molecular ions. Samples were introduced directly to the ESI source at a flow rate of 3 μ L min⁻¹. The ion accumulation time was varied, from 0.1 to 0.5 s, to account for differences in carbon (C) concentration between samples. The instrument was externally calibrated weekly with a tuning solution from Agilent (Santa Clara, CA), which calibrates to a mass accuracy of < 0.1 ppm. Two hundred scans were averaged for each sample and internally calibrated using the homologous series of organic molecules separated by 14 Da ($-CH_2$ groups). The mass measurement accuracy was less than 1 ppm for singly charged ions across a broad m/z range (*i.e.*, 200 < m/z < 1200). To further reduce cumulative errors, all sample peak lists for the entire dataset were aligned to each other prior to formula assignment to eliminate possible mass shifts that would impact formula assignment. Putative chemical formulas were assigned using Formularity software⁵⁵. Chemical formulas were assigned based on the following criteria: signal to noise ratio (S/N) > 7, and mass measurement error < 1 ppm, taking into consideration the presence of C, H, O, N, S and P and excluding other elements. Peaks with large mass ratios (m/z values > 500 Da) were assigned formulas through the detection of homologous series (CH_2 , O, H_2). Additionally, to ensure consistent assignment of molecular formulas, the following rules were implemented: one phosphorus requires at least four oxygens in a formula, and when multiple formula candidates were assigned the formula with the lowest error and with the lowest number of heteroatoms was picked. The molecular formulas were grouped based on heteroatom composition: CHO, CHON, CHOS, CHOP, CHONS, CHONP, and CHONSP. Further, the molecular formulas were also tentatively grouped into eight compound classes based on elemental stoichiometries: condensed aromatic compounds, unsaturated hydrocarbons, tannins, lignin/carboxyl-rich alicyclic molecules (CRAM), lipids, proteins, amino sugars, and carbohydrates (according to Tfaily et al. 2015) (criteria detailed in **Table S2**). It is important to note that CRAM fits within the van Krevelen space labeled “lignin-like”. Assignments of molecular formulas to compound classes are tentative

1
2
3 because structural information cannot be gained from molecular stoichiometries alone.
4 Additional analysis is required to tease apart whether lignin and/or CRAM exist in the samples.
5 As such, we included both identifications in the discussion. From the formula assignment,
6 the average (by number-weighted) abundance of each class was calculated and compared
7 between samples ⁵⁶. The relative abundance of molecules based on heteroatom content
8 and compound classification are presented in **Table S3 and S4**, respectively. The
9 molecular properties (*e.g.*, molecular weight, O/C, and O/H) of the NOM samples were
10 calculated from the assigned molecular formulas and are summarized in **Table S5**.
11
12
13
14
15
16
17
18
19

20 ***Aggregation of PVP-PtNPs***

21
22 The aggregation behavior of PVP-PtNPs (PtNP₂₀-PtNP₉₅) was determined by
23 monitoring the evolution of PVP-PtNP number size distribution and number and mass
24 concentrations by sp-ICP-MS after (*e.g.*, 0 and 24 h) mixing 1 $\mu\text{g L}^{-1}$ PVP-PtNPs with
25 UPW and moderately hard water (MHW; composition detailed in **Table S6**). The effect
26 of NOM on the aggregation of PVP-PtNPs in MHW was determined after mixing 1 μg
27 L^{-1} PVP-PtNPs (PtNP₂₀ and PtNP₉₅) with MHW in the presence of 1 mg L^{-1} NOM under
28 static conditions. All aggregation experiments were conducted in triplicate. We present
29 the average of experimental triplicate measurements for the number and mass
30 concentrations and the number-average diameter values. All sp-ICP-MS data were
31 acquired with a NexION™ 350D ICP-MS (PerkinElmer Inc., MA, USA) operating in a
32 single particle mode with the Syngistix Nano Application Module. A standard
33 introduction system was used consisting of a Meinhard glass concentric nebulizer, a glass
34 cyclonic spray chamber, and a 2 mm inner-diameter quartz injector. The sample uptake
35 rates were 0.28-0.32 mL min^{-1} . Data were acquired at an RF power of 1600 W, a 50 μs
36 dwell time, a 0 μs settling time, and a 60 s acquisition time. The transport efficiencies
37 were 9.6-12.7%. NIST™ Au standard reference material (actual TEM size of 56 nm;
38 reference material 8013 manufactured by National Institute of Standard and Technology,
39 MD, USA) was used to determine the transport efficiency. A rinse cycle, consisting of 1
40 min with 1% aqua regia and 1 min with UPW, was performed after each sample run to
41 ensure cleansing of the sample introduction system between samples. The NIST Au
42 standard reference material was measured after each set as a QA/QC check.
43
44
45
46
47
48
49
50
51
52
53
54
55
56
57
58
59
60

Statistical analysis

Statistical analyses were performed with SAS[®] version 9.4 software (SAS institute, Cary, NC). Correlation coefficients between the percentage of mass of aggregated NPs and the NOM elemental composition and properties were calculated using Pearson's correlation method. Calculated Pearson's correlation coefficient (r) and p -values (**Table 1**) were used to assess the correlation quality with each NOM parameter. The percentage of mass of aggregated NPs in the presence of six NOM samples and a control (without NOM) were analyzed using ANOVA and Tukey's multiple comparison test. Particle size distribution of PVP-PtNPs in the absence and presence of different NOM samples were analyzed using Kolmogorov-Smirnov (K-S) test with Bonferroni correction. In all cases, the statistical significance was set at p -value < 0.05 .

RESULTS AND DISCUSSIONS

NOM characterization

The number-average molecular weight and SUVA₂₅₄ values of the HPOA fractions of NOM samples varied between 369-442 Da and 0.8-4.8 L mg⁻¹ m⁻¹, respectively (**Tables S1 and S6**). The N and S content of the NOM samples varied significantly (0.8-1.8% and 0.4-1.9%, respectively; **Table S1**). CHO and CHON were the main classes of compounds when grouped by heteroatom composition ($> 5\%$ of total formulas), and displayed a notable variation between the six NOM samples (**Table S3**). CHOS and CHONS were generally less abundant (1.6 to 7.5% and 1.9 to 8.1% of total formulas, respectively) with select NOM samples (NOM 1, 2 and 5) containing $> 5\%$ of these two classes of compounds, and the abundance of these formulas largely following elemental S and N content (**Table S1**). Heteroatom classes of compounds including P (*e.g.*, CHOP, CHONP, CHONSP, and others) represented only $< 5\%$ of all formulas in all NOM samples. Condensed hydrocarbon-, lignin-/CRAM-, and tannin-like compounds were the main chemical classes of compounds in NOM and varied significantly between the six NOM samples (**Table S4**). Other molecules assigned to compound classes (*e.g.*, aminosugar, carbohydrates, lipid, unsaturated hydrocarbons, and others) represented $< 5\%$ of all formulas in all NOM samples. It is important to recognize that the type of sorbent used for solid-phase extraction of NOM influences the molecular diversity as

determined by FTICR-MS⁵⁷. The number average elemental ratio of O/C and H/C varies within a narrow range (0.48-0.52 and 1.05-1.26, respectively, **Table S5**) between the different NOM samples. Collectively, the observed differences in the bulk elemental composition, SUVA₂₅₄, and molecular properties of NOM samples reflect differences in NOM source and environmental processing (**Table S1**), rather than ionization and detection variations in the measurement technique as all samples were analyzed using the same protocol and at the same time.

Particle characterization

TEM micrographs show that the synthesized PVP-PtNPs are spherical (**Figure S1**). PtNP₂₀, PtNP₃₀, PtNP₇₅, and PtNP₉₅ exhibited monomodal PSDs, whereas PtNP₅₀ exhibited a bimodal PSD (**Figure 1a**). The mean core diameters of PtNP₂₀, PtNP₃₀, PtNP₅₀, PtNP₇₅, and PtNP₉₅ measured by TEM are 9.2±1.2, 10.9±0.8, 18.5±5, 44.5±5, and 72.5±3.9 nm, respectively (**Table S7**). sp-ICP-MS analysis show that all PVP-PtNPs exhibited monomodal PSDs, with mean core diameters for PtNP₂₀-PtNP₉₅ of 26.4 ± 11.6, 30.2 ± 12.9, 34.3 ± 10.1, 44.1 ± 7.7, and 76.7 ± 9.7 nm, respectively (**Figure 1b, Table S8**). The mean core diameters for PVP-PtNP₇₅ and PVP-PtNP₉₅ measured by sp-ICP-MS are in good agreement with those measured by TEM (**Table S7**). However, the mean core diameters of PVP-PtNP₂₀, PVP-PtNP₃₀, and PVP-PtNP₅₀ measured by sp-ICP-MS were larger than those measured by TEM (**Table S7**). These size differences can be attributed to the greater size detection limit of sp-ICP-MS for PVP-PtNP (*e.g.*, 18 nm⁵⁸) compared to TEM (*e.g.*, typically < 1 nm, depending on the TEM spectrum and operating condition⁵⁹). The PSDs of PVP-PtNP₂₀, PVP-PtNP₃₀, and PVP-PtNP₅₀ obtained by sp-ICP-MS are monomodal but represent curtailed log-normal size distribution, resulting in greater mean core sizes compared to those measured by TEM.

The number concentration of PVP-PtNP₂₀, PVP-PtNP₃₀, and PVP-PtNP₅₀ in UPW measured by sp-ICP-MS represents a small fraction (*e.g.*, 0.3, 1.2, and 33.1%, respectively) of the theoretical particle number concentration (**Table S8**). In contrast, the measured number concentrations of PVP-PtNP₇₅ and PVP-PtNP₉₅ in UPW were in good agreement with the theoretical number concentration (**Table S8**). This is attributed to the size detection limit of sp-ICP-MS⁵⁸. The number PSD measured by TEM illustrates that all NPs in PVP-PtNP₂₀, and PVP-PtNP₃₀ and 54% of NPs in PVP-PtNP₅₀ are below the

sp-ICP-MS size detection limit, whereas all particles in PVP-PtNP₇₅ and PVP-PtNP₉₅ are larger than the sp-ICP-MS size detection limit for PtNPs (**Figure 1b**).

The zeta potential of the synthesized PVP-PtNPs decreased from -16.9 ± 3.5 to -27.2 ± 1.7 with the increase in particle size (**Table S7**), which might be attributed to the partial coating of PtNPs. Typically, NPs fully coated with PVP molecules exhibit low zeta potential of approximately -10 mV^{60, 61}. Higher zeta potential of PVP-coated NPs has been reported elsewhere and was attributed to the partial surface coating of NPs by PVP molecules⁶²⁻⁶⁴. For instance, the magnitude of the zeta potential of PVP-partially coated AgNPs increased with a decrease in the number of PVP molecules per AgNP unit surface area².

Size-dependent aggregation of PVP-PtNPs

The number PSDs of PVP-PtNP₂₀ – PVP-PtNP₇₅ exhibited a modest shift towards larger sizes immediately after mixing with MHW (0 h) relative to the corresponding PSDs of PVP-PtNP₂₀ – PVP-PtNP₇₅ measured in UPW (**Figure 2a-d**). After 24 h in MHW, the PSDs of PVP-PtNP₂₀ – PVP-PtNP₇₅ shifted further towards larger sizes, which indicates PVP-PtNP aggregation in MHW. The aggregation of PVP-PtNPs in MHW relative to UPW can be attributed to the higher ionic strength of the MHW which screens the PVP-PtNP surface charge. The magnitude of the zeta potential of each PVP-PtNP suspension (1 mg L^{-1}) decreased in MHW at 0 h and further decreased at 24 h relative to the corresponding zeta potential measured in UPW (**Table S9**). The number PSD of PVP-PtNP₉₅ did not change in MHW relative to that measured in UPW (**Figure 2e**), indicating that PVP-PtNP₉₅ are stable in MHW.

The number concentrations of PVP-PtNP₂₀ and PVP-PtNP₃₀ increased immediately after mixing with MHW relative to those measured in UPW and increased further after 24 h (**Table S8**). This observation is counterintuitive, as one would expect NP number to decrease with NP aggregation. However, due to aggregation, PVP-PtNP aggregate size became larger than the size detection limit of sp-ICP-MS for PtNPs (*i.e.*, 18 nm). Thus, NP aggregation increased the detectable PtNPs by sp-ICP-MS and increased the measured PVP-PtNP number concentration (**Table S8 and Figure 2a-b**). This is corroborated by the increase in mass concentration of PVP-PtNP₂₀ and PVP-PtNP₃₀ measured by sp-ICP-MS in MHW relative to those measured in UPW (**Table S10**).

1
2
3 The number concentration of PVP-PtNP₅₀ and PVP-PtNP₇₅ decreased
4 immediately after mixing with MHW relative to the number concentration in UPW and
5 decreased further after 24 h of mixing with MHW (**Table S8**), which can be attributed to
6 particle aggregation. Aggregation of PVP-PtNP₅₀ should increase the number particle
7 concentration, as observed for PVP-PtNP₂₀ and PVP-PtNP₃₀. However, only 33% of NPs
8 in PVP-PtNP₅₀ were smaller than the sp-ICP-MS size detection limit. Thus, aggregation
9 of PVP-PtNP₅₀ increases the size of undetectable particles to become detectable and thus
10 increase the number particle concentration, but aggregation also reduces the number of
11 NPs larger than the sp-ICP-MS detection limit. Thus, the measured number concentration
12 is influenced by these two counteracting processes. All NPs in PVP-PtNP₇₅ were larger
13 than the size detection limit of sp-ICP-MS and thus the number concentration of PVP-
14 PtNP₇₅ in MHW decreased relative to that in UPW due to particle aggregation. The
15 number concentrations of PVP-PtNP₉₅ in UPW and in MHW at t= 0 were not statistically
16 different ($p < 0.05$) (**Table S8**). The number concentration of PVP-PtNP₉₅ in MHW
17 decreased (*e.g.*, 35% reduction, **Table S8**) after 24 h in MHW, but the number PSD of
18 PVP-PtNP₉₅ did not change after 24 h in MHW. This might be due to the aggregation of
19 some PVP-PtNPs without a significant shift in the number PSD, or to sedimentation of
20 some PVP-PtNPs, or to both processes. Nevertheless, the decrease in PVP-PtNP₇₅ and
21 PVP-PtNP₉₅ mass concentration suggest a loss of some PVP-PtNPs, most likely due to
22 PVP-PtNP sedimentation. Sedimentation of PVP-PtNP₇₅ and PVP-PtNP₉₅ was observed
23 in the stock suspensions within 24-48 h, mainly because of the high density of PtNPs
24 (21.45 g cm⁻³). Similar gravitational sedimentation of 65 and 87.5 nm AuNPs (density =
25 19.32 g cm⁻³) in UPW under static condition was observed after 48 h ⁶⁵.

26
27
28
29
30
31
32
33
34
35
36
37
38
39
40
41
42
43 The number PSD of PVP-PtNP₂₀ and PVP-PtNP₃₀ 24 h after mixing with MHW
44 (**Figure 2a and b**) exhibited broader size distributions compared to PVP-PtNP₅₀, PVP-
45 PtNP₇₅, and PVP-PtNP₉₅ (**Figure 2c, d, and e**). This observation indicates that smaller
46 PVP-PtNPs are more prone to aggregation and form larger aggregates compared those
47 formed by the aggregation of larger PVP-PtNPs. This is consistent with previous studies
48 demonstrating an increased aggregation of smaller hematite NPs ³, TiO₂ NPs ^{4, 66}, and cit-
49 PtNPs under the same experimental conditions relative to their larger counterpart ⁷. NP
50 aggregation occurs because of NP collision and attachment. Collision increases with the
51 increase in NP number concentration, whereas attachment increases with the decrease in
52 NP zeta potential. At the same mass concentration, NP number concentration increases
53
54
55
56
57
58
59
60

1
2
3 with the decrease in NP size. The magnitude of zeta potential decreases with decreasing
4 NP size (**Table S9**). Thus, both factors (zeta potential, NP number concentration)
5 contribute to the increased aggregation with decreasing PVP-PtNP sizes. However,
6 positive correlation ^{2, 5} and insignificant correlation ⁶ between primary particle size and
7 aggregation were also reported in literature. The detection of small particles in PVP-
8 PtNP₂₀, PVP-PtNP₃₀, and PVP-PtNP₅₀ suspensions (**Figure 2a, b, and c**) after 24 h in
9 MHW that were not detected in the corresponding suspensions in UPW is attributed to
10 the aggregation of PVP-PtNPs that are smaller than the sp-ICP-MS size detection limit in
11 MHW.
12
13
14
15
16
17
18
19
20
21

22 *NOM-dependent aggregation of PVP-PtNPs*

23
24 The PSDs of PVP-PtNP₂₀ (1 µg L⁻¹) in MHW in the presence of NOM (1 mg L⁻¹)
25 samples at time 0 h were not statistically different (Kolmogorov-Smirnov test; *p*-value >
26 0.065) than the PSD of PVP-PtNP₂₀ measured in MHW (without NOM) at time 0 h
27 (**Figure 3**), suggesting a lack of immediate aggregation of PVP-PtNP₂₀ in MHW in the
28 presence of NOM. After 24 h, the PSDs of PVP-PtNP₂₀ in the presence of NOM samples
29 shifted toward larger sizes relative to the measured PSD at time 0 h, indicating
30 aggregation of PVP-PtNP₂₀ in MHW in the presence of all NOM samples after 24 hours.
31 Whereas the PSD of PVP-PtNP₂₀ after 24 hours mixing in MHW displayed a bimodal
32 distribution (**Figure 2a**), the PSDs of PVP-PtNP₂₀ in the presence of the different NOMs
33 exhibited monomodal distributions (**Figure 3**). The PSDs of PVP-PtNP₂₀ in presence of
34 NOM 1, 2, 3, 5, and 6 after 24 h in MHW were not statically different (Kolmogorov-
35 Smirnov test; *p* > 0.4) relative to the PSD of PVP-PtNP₂₀ after 24 h in MHW without
36 NOM. However, the PSDs of PVP-PtNP₂₀ in presence of NOM 4 after 24 h in MHW was
37 statically different (larger, Kolmogorov-Smirnov test; *p* < 0.05) relative to the PSD of
38 PVP-PtNP₂₀ after 24 h in MHW without NOM. Similarly, the mean number diameters of
39 PVP-PtNP₂₀ in the presence of NOM 1, 2, 3, 5 and 6 (**Table S11**), were not significantly
40 different (t-test; *p* > 0.05) relative to the mean diameter of PVP-PtNP₂₀ after 24 h in MHW
41 without NOM. In contrast, the mean diameter of PVP-PtNP₂₀ in presence of NOM 4
42 (Pacific Ocean HPOA) was larger than the mean diameter of PVP-PtNP₂₀ in MHW
43 without NOM and in MHW in presence of all other NOM samples (t-test; *p* < 0.05). These
44 results suggest that NOM differently impacted PVP-PtNP₂₀ aggregation and stability.
45
46
47
48
49
50
51
52
53
54
55
56
57
58
59
60

1
2
3 To evaluate PVP-PtNPs aggregation in the absence and presence of NOM, the
4 number and mass concentrations of PVP-PtNPs measured by sp-ICP-MS were compared
5 to the theoretical number and mass concentrations, respectively. The number
6 concentration of PVP-PtNP₂₀ after mixing with MHW in presence of NOM samples
7 increased from <1 % at 0 h to 11-52% at 24 h of the theoretical PVP-PtNP₂₀ number
8 concentration, respectively (**Table S11**), confirming the aggregation of PVP-PtNP₂₀ in
9 MHW in presence and/or absence of NOM. In contrast, PVP-PtNP₂₀ in UPW did not
10 aggregate during 24 h exposure and the number concentration of PVP-PtNP₂₀ remained
11 constant and represented only 0.7% of the theoretical PVP-PtNP₂₀ concentration. The
12 mass concentration of PVP-PtNP₂₀ in the presence and absence NOM samples also
13 followed the same trend. The mass concentration of PVP-PtNP₂₀ after mixing with MHW
14 in presence of NOM samples increased from <4% 0h to 19 to 98% at 24 of the theoretical
15 PVP-PtNP₂₀ mass concentration (**Table S12**).

16
17 The number concentration of PVP-PtNP₂₀ in presence of NOM 4 was significantly
18 higher than the number concentration of PVP-PtNP₂₀ in absence of NOM (**Figure 4a**; p
19 < 0.05), whereas the number concentration of PVP-PtNP₂₀ in presence of NOM 1, 2, 3,
20 5, and 6 were not significantly different compared to the number concentration of PVP-
21 PtNP₂₀ in absence of NOM (**Figure 4a**; ANOVA with Tuckey's multiple comparison
22 test; $\alpha= 0.05$). The mass concentration of PVP-PtNP₂₀ in presence of NOM 4 was larger
23 than the mass concentration of PVP-PtNP₂₀ in absence of NOM and in presence all other
24 NOM samples. However, the mass concentration of PVP-PtNP₂₀ in presence of NOM 1,
25 2, 3, 5, and 6 were not significantly different relative to the mass concentration of PVP-
26 PtNP₂₀ in absence of NOM (**Figure 4b**; ANOVA with Tuckey's multiple comparison; $\alpha=$
27 0.05). The mass concentration of PVP-PtNP₂₀ in presence of NOM 1 was lower than the
28 mass concentration of PVP-PtNP₂₀ in presence of NOM 2 (ANOVA with Tuckey's
29 multiple comparison test; $\alpha= 0.05$), whereas the mass concentration of PVP-PtNP₂₀ in the
30 presence of NOM 2, 3, 5 and 6 were not significantly different among themselves. These
31 results indicate that NOM 4 influenced PVP-PtNP₂₀ aggregation differently than all other
32 NOM samples. Below we discuss how the molecular composition and properties of the
33 NOM samples help explain differences in how NOM affects PVP-PtNP₂₀ aggregation.

34
35 We interpret the increased aggregation of PVP-PtNP₂₀ in the presence of NOM to
36 be a result of inter-particle bridging of NOM-coated PVP-PtNPs due to complex
37 formation between humic acid macromolecules and divalent counterions (*e.g.*, Ca²⁺ and
38
39
40
41
42
43
44
45
46
47
48
49
50
51
52
53
54
55
56
57
58
59
60

1
2
3 Mg^{2+}). This is agreement with the bridging of PVP-AuNPs in the presence of NOM and
4 high concentrations of Ca^{2+} and Mg^{2+} ⁶⁷. The concentrations of monovalent counterions
5 in MHW (*e.g.*, 1.14 mM Na^+ and 0.05 mM K^+ , **Table S3**) are lower than that (*e.g.*, ≥ 50
6 mM Na^+) required to initiate PVP-PtNP₂₀ aggregation ⁷. However, the concentrations of
7 divalent counterions in MHW (*e.g.*, 0.45 mM Ca^{2+} and 0.5 mM Mg^{2+} , **Table S6**) are in
8 close proximity to the critical coagulation concentration (*e.g.*, 1.1 Ca^{2+}) for PVP-PtNP₂₀
9 and thus can result in a significant aggregation of PVP-PtNP₂₀ ⁷. However, this bridging
10 phenomenon may depend on the type, composition and structure of the NOM, which has
11 not been investigated previously.
12

13
14
15
16
17
18
19 The PSD of PVP-PtNP₉₅ in MHW in the presence of NOM samples at 0 and 24 h
20 (**Figure 5**) were not statistically different from those measured in MHW at time 0 h or 24
21 h (**Figure 2e**). This observation indicates that all NOM samples did not have significant
22 impact on the colloidal stability of PVP-PtNP₉₅. The number concentration of PVP- PVP-
23 PtNP₉₅ decreased slightly in MHW relative to that measured in UPW at 24 h (**Table S13**),
24 indicating slight particle aggregation and/or sedimentation. The mass concentration of
25 PVP-PtNP₉₅ decreased slightly in MHW relative to that measured in UPW at 24 h (**Table**
26 **S14**) indicating modest particle aggregation and/or sedimentation of PVP-PtNPs during
27 this period. The number and mass concentrations of PVP-PtNP₉₅ in MHW increased
28 slightly in the presence of all NOM samples relative to treatments without NOM,
29 suggesting that the presence of NOM enhanced the stability of PVP-PtNP₉₅.
30
31
32
33
34
35
36
37

38 Taken together, these results suggest that the effect of NOM on PVP-PtNP
39 aggregation is size-dependent. The stability of smaller PVP-PtNPs appeared more
40 influenced by NOM than that of the larger PVP-PtNPs, which might be attributed to the
41 size-dependent NOM-corona composition/properties. For instance, Pettibone et al (2008)
42 demonstrated differences in adsorption sites or the distribution of adsorption sites for
43 oxalic acid on the surfaces of 5 nm and 32 nm TiO_2 -NPs, which was attributed to greater
44 abundance of lower energy binding sites, associated with edge and corner sites, available
45 for adsorption of oxalic acids on the surfaces of 5 nm TiO_2 -NPs compared to that on the
46 surfaces of 32 nm TiO_2 -NPs ⁶⁶. Differences in adsorption sites on NP surfaces can be
47 even more important for the adsorption of NOM on NP surfaces due to polydiversity of
48 NOM formulas. Zhang et al. (1999) reported increased adsorption of organic acids with
49 decreasing (*e.g.*, 6-16 nm) TiO_2 NP sizes ⁶⁸. Smaller particles with increased molar free
50 energy are more prone to adsorb molecules or ions per unit area onto their surfaces in
51
52
53
54
55
56
57
58
59
60

1
2
3 order to decrease the total free energy and become more stable⁶⁸. Chowdhury et al. (2013)
4 reported that NOM affect the morphology of TiO₂ NP aggregates, where small NPs (*e.g.*,
5 6 nm) form more compact aggregates than larger NPs in the presence of NOM (*e.g.*, 13
6 nm and 23), suggesting that interactions of NOM with smaller NPs are more significant
7 than those with larger ones⁷⁷. At a fixed mass concentration, larger NPs display a smaller
8 total surface area (**Table S8**). Therefore, at a fixed NOM concentration, higher number
9 of NOM molecules are available for interaction with larger NP surfaces per unit surface
10 area. This may enhance the stability of larger particles compared to that of smaller NPs
11 in the presence of NOMs.
12
13
14
15
16
17
18
19

20 ***Correlating PVP-PtNP₂₀ aggregation to NOM molecular properties***

21
22 The NOM samples used in this study represents a diverse array of NOM
23 compositional differences relevant to all aquatic systems. Differences in NOM
24 composition among samples may explain the variation in the observed particle
25 aggregation. To identify the NOM properties with the greatest influence on NP
26 aggregation, we performed Pearson's correlation analysis between mass of aggregated
27 PVP-PtNP₂₀ and specific NOM properties. PVP-PtNP₉₅ were not included in these
28 correlation analysis as they did not exhibit any appreciable aggregation in the presence or
29 absence of NOM.
30
31
32
33
34
35

36 Bulk and molecular-level properties of NOM samples provided robust prediction
37 of the aggregation of PVP-PtNP₂₀. Negative correlations of statistical significance were
38 observed between the mass of aggregated PVP-PtNP₂₀ and NOM MW ($r = -0.979$, $p =$
39 0.004), SUVA₂₅₄ ($r = -0.763$, $p = 0.078$), O/C ratio ($r = -0.841$, $p = 0.036$), relative
40 abundance of condensed hydrocarbons (ConHC, $r = -0.766$, $p = 0.076$), and relative
41 abundance of tannin molecules ($r = -0.898$, $p = 0.015$). Positive correlations of statistical
42 significance were observed between the mass of aggregated PVP-PtNP₂₀ and NOM H/C
43 ($r = 0.73$, $p = 0.1$) and relative abundances of lignin/CRAM ($r = 0.798$, $p = 0.058$) (**Table**
44 **1, S4-S6 and Figure 6, Figure S3**).
45
46
47
48
49
50

51 Correlations between PVP-PtNP₂₀ aggregation and NOM properties are
52 interpreted to reflect differences in molecular hydrophobicity and charge density.
53 Aggregation of PVP-PtNP₂₀ was limited in the presences of NOM that was more
54 hydrophobic, as measured by SUVA₂₅₄ (**Figure 6b**), abundance of condensed
55 hydrocarbon (**Figure 6c**), and H/C, a measure of hydrogen saturation (**Figure S3e**). NOM
56
57
58
59
60

1
2
3 samples with higher $SUVA_{254}$ and relative abundance of ConHC are expected to result in
4 higher sorption of these molecules on NP surfaces and thus increasing the NP
5 hydrophobicity, and thus may enhance repulsive forces between NPs. NOM samples with
6 higher average MW, which also co-varies with aromaticity⁶⁹, would presumably lead to
7 thicker adsorbed layers of NOM on NP surfaces, resulting in increased steric
8 stabilization⁷⁰⁻⁷². Aggregation of PVP-PtNP₂₀ was also influenced by the charge density
9 of the NOM, as measured principally by the O/C (**Figure S3d**). NOM sample with higher
10 O/C, and thus higher charge density, demonstrated negative correlation with the observed
11 aggregation (**Table 1**). In contrast, NOM samples with lower charge density parameters
12 (*i.e.*, low O/C) showed positive correlation with the aggregated mass (**Table 1**). Higher
13 oxygen content and O/C ratio indicates a higher content of functional groups such as
14 carboxylic and carbonyl groups²⁶. The higher content of these functional groups is likely
15 to enhance NP surface charge, which increases the electrostatic repulsive forces between
16 NOM-coated PVP-PtNPs, and thus enhances NP stability²⁶. In summary, aggregation of
17 PVP-PtNPs is interpreted to be a function of both the NOM hydrophobicity and charge
18 density, and the selective sorption of NOM molecules to NP surfaces that control NP
19 stability⁷³⁻⁷⁸. Similar observations have been made for ZnS NPs²⁶ and cit-AuNPs²⁴.
20 Thus, larger MW, higher $SUVA_{254}$, and relative abundance of ConHC in NOM samples
21 enhance NP₂₀ stability^{24, 26}.

22
23
24
25
26
27
28
29
30
31
32
33
34
35
36 NOM molecules with high O/C (*i.e.*, tannin) demonstrated significant negative
37 correlation, whereas those with lower O/C (*i.e.*, lignin/CRAM, conHC etc.) demonstrated
38 significant positive correlation with the mass of aggregated PVP-PtNP₂₀, in good
39 agreement with the correlations observed with O/C ratios as discussed above.
40 Lignin/CRAM- and tannin- like compounds contain the same types of surface functional
41 groups (hydroxyl, carbonyl groups and phenol groups). However, tannins are high
42 molecular weight polycyclic aromatic compounds with high O/C ratio and charge density
43 than CRAM molecules, which is likely to enhance the NP surface charge, and thus, result
44 in higher NP stability. Additionally, the hydrophobic nature and polymer structure of
45 tannins might be responsible for increased NP stability and decreased aggregation⁷⁹.
46 Lignin/CRAM are high molecular polyphenolic compounds⁷⁹. These poly-phenol
47 compounds have particular importance as they promote aggregation by forming strong
48 non-covalent bonds⁸⁰. Lignin/CRAM have hydrophilic regions such as hydroxyls (–OH),
49 carboxylic (–COOH) and small alkyl chains *i.e.*, methane groups (–CH₃). These
50
51
52
53
54
55
56
57
58
59
60

1
2
3 functional groups and the hydrophobic regions of lignin/CRAM (*e.g.*, resinol, C-H
4 groups) enable it to bind with nanoparticle surfaces through polar, covalent, and hydrogen
5 bonding as well as Van der Waals forces. These humidified and highly decomposed
6 materials, which are more stable, aid in the formation of microaggregates⁸¹. For instance,
7 lignin has been shown to promote macroaggregation in soil and to increase aggregate
8 stability⁸¹⁻⁸³.
9
10
11
12
13
14

15 **Conclusions**

16
17 This study demonstrated that aggregation of PVP-PtNPs depend on several
18 factors, including NP size and NOM characteristics. At the same mass concentration,
19 PVP-PtNP aggregate size increased with the decrease in NP primary size due to the
20 increased NP number concentration and therefore collision frequency. NOM samples of
21 different compositions and properties did not alter the aggregation behavior of PVP-
22 PtNP₉₅ in MHW. However, the same NOM samples generally increased the aggregation
23 of PVP- PVP-PtNP₂₀ in MHW to different extents, likely via bridging mechanism(s) in
24 the presence of divalent counterions in MHW. The mass of aggregated PVP-PtNP₂₀
25 decreased with the increase in NOM elemental ratio of O/C, molecular weight, SUVA₂₅₄,
26 and relative abundance of condensed hydrocarbons and tannin. The mass of the
27 aggregated PVP-PtNP₂₀ increased with the increase in NOM elemental ratio of H/C and
28 the relative abundance of lignin/CRAM formulas. Therefore, the molecular composition
29 and properties, and thus sources, of NOM may determine to a great extent PVP-PtNP
30 colloidal stability in aquatic environments.
31
32
33
34
35
36
37
38
39
40

41 Future studies are needed to unravel the complex and subtle impacts of NOM
42 composition and properties on NP stability. Specifically, information is needed on NP
43 stability under various conditions of NOM concentration (*e.g.*, 1 to 30 mg C L⁻¹), NP
44 concentration (*e.g.*, µg L⁻¹ to mg L⁻¹) and properties (*e.g.*, size, shape, and surface
45 coating), water physicochemical properties (*e.g.*, pH, ionic strength and composition),
46 presence of suspended particulate matter, water dynamics (*e.g.*, static *vs.* stirring, or water
47 turbulence), and aging time (*e.g.*, weeks and months). Future efforts on the stability of
48 PtNPs and that of other NPs is needed to develop quantitative structure activity
49 relationships between NOM molecular properties and the environmental behaviors of
50 NPs.
51
52
53
54
55
56
57
58
59
60

Acknowledgment

This work was supported by US National Science Foundation NSF-EPSCoR Fellowship (1738340) to Dr. Mohammed Baalousha. A portion of this research was performed using EMSL, a DOE Office of Science User Facility sponsored by the Office of Biological and Environmental Research. Any use of trade, firm, or product names is for descriptive purposes only and does not imply endorsement by the U.S. Government.

Reference

1. Baalousha, M., Effect of nanomaterial and media physicochemical properties on nanomaterial aggregation kinetics. *NanoImpact* **2017**, *6*, 55-68.
2. Afshinnia, K.; Sikder, M.; Cai, B.; Baalousha, M., Effect of nanomaterial and media physicochemical properties on Ag NM aggregation kinetics. *Journal of Colloid and Interface Science* **2017**, *487*, 192-200.
3. He, Y. T.; Wan, J.; Tokunaga, T., Kinetic stability of hematite nanoparticles: the effect of particle sizes. *Journal of Nanoparticle Research* **2008**, *10* (2), 321-332.
4. Zhou, D.; Ji, Z.; Jiang, X.; Dunphy, D. R.; Brinker, J.; Keller, A. A., Influence of Material Properties on TiO₂ Nanoparticle Agglomeration. *PLOS ONE* **2013**, *8* (11), e81239.
5. Mulvihill, M. J.; Habas, S. E.; Jen-La Plante, I.; Wan, J.; Mokari, T., Influence of Size, Shape, and Surface Coating on the Stability of Aqueous Suspensions of CdSe Nanoparticles. *Chemistry of Materials* **2010**, *22* (18), 5251-5257.
6. Liu, J.; Legros, S.; Ma, G.; Veinot, J. G. C.; von der Kammer, F.; Hofmann, T., Influence of surface functionalization and particle size on the aggregation kinetics of engineered nanoparticles. *Chemosphere* **2012**, *87* (8), 918-924.
7. Sikder, M.; Wang, J.; Chandler, G. T.; Berti, D.; Baalousha, M., Synthesis, characterization, and environmental behaviors of monodispersed platinum nanoparticles. *Journal of Colloid and Interface Science* **2019**, *540*, 330-341.
8. Leenheer, J. A.; Croue, J. P., Characterizing aquatic dissolved organic matter. *Environ Sci Technol* **2003**, *37* (1), 18a-26a.
9. Nebbioso, A.; Piccolo, A., Molecular characterization of dissolved organic matter (DOM): a critical review. *Analytical and Bioanalytical Chemistry* **2013**, *405* (1), 109-124.
10. Spencer, R. G. M.; Butler, K. D.; Aiken, G. R., Dissolved organic carbon and chromophoric dissolved organic matter properties of rivers in the USA. *Journal of Geophysical Research: Biogeosciences* **2012**, *117* (G3).
11. Keller, A. A.; Wang, H.; Zhou, D.; Lenihan, H. S.; Cherr, G.; Cardinale, B. J.; Miller, R.; Ji, Z., Stability and Aggregation of Metal Oxide Nanoparticles in Natural Aqueous Matrices. *Environmental Science & Technology* **2010**, *44* (6), 1962-1967.
12. Petosa, A. R.; Jaisi, D. P.; Quevedo, I. R.; Elimelech, M.; Tufenkji, N., Aggregation and Deposition of Engineered Nanomaterials in Aquatic Environments:

1
2
3 Role of Physicochemical Interactions. *Environmental Science & Technology* **2010**, *44*
4 (17), 6532-6549.

5
6 13. Gu, B.; Schmitt, J.; Chen, Z.; Liang, L.; McCarthy, J. F., Adsorption and
7 desorption of different organic matter fractions on iron oxide. *Geochimica et*
8 *Cosmochimica Acta* **1995**, *59* (2), 219-229.

9
10 14. Gibson, C. T.; Turner, I. J.; Roberts, C. J.; Lead, J. R., Quantifying the
11 Dimensions of Nanoscale Organic Surface Layers in Natural Waters. *Environmental*
12 *Science & Technology* **2007**, *41* (4), 1339-1344.

13
14 15. Lynch, I.; Dawson, K. A.; Lead, J. R.; Valsami-Jones, E., Chapter 4-
15 macromolecular coronas and their importance in nanotoxicology and nanoecotoxicology.
16 *Front Nanosci* **2014**, *7*.

17
18 16. Lau, B. L. T.; Hockaday, W. C.; Ikuma, K.; Furman, O.; Decho, A. W., A
19 preliminary assessment of the interactions between the capping agents of silver
20 nanoparticles and environmental organics. *Colloids and Surfaces A: Physicochemical*
21 *and Engineering Aspects* **2013**, *435*, 22-27.

22
23 17. Diegoli, S.; Manciuola, A. L.; Begum, S.; Jones, I. P.; Lead, J. R.; Preece, J. A.,
24 Interaction between manufactured gold nanoparticles and naturally occurring organic
25 macromolecules. *Science of The Total Environment* **2008**, *402* (1), 51-61.

26
27 18. Gondikas, A. P.; Morris, A.; Reinsch, B. C.; Marinakos, S. M.; Lowry, G. V.;
28 Hsu-Kim, H., Cysteine-Induced Modifications of Zero-valent Silver Nanomaterials:
29 Implications for Particle Surface Chemistry, Aggregation, Dissolution, and Silver
30 Speciation. *Environmental Science & Technology* **2012**, *46* (13), 7037-7045.

31
32 19. Mohd Omar, F.; Abdul Aziz, H.; Stoll, S., Aggregation and disaggregation of
33 ZnO nanoparticles: Influence of pH and adsorption of Suwannee River humic acid.
34 *Science of The Total Environment* **2014**, *468-469*, 195-201.

35
36 20. Ghosh, S.; Jiang, W.; McClements, J. D.; Xing, B., Colloidal Stability of
37 Magnetic Iron Oxide Nanoparticles: Influence of Natural Organic Matter and Synthetic
38 Polyelectrolytes. *Langmuir* **2011**, *27* (13), 8036-8043.

39
40 21. Loosli, F.; Le Coustumer, P.; Stoll, S., TiO₂ nanoparticles aggregation and
41 disaggregation in presence of alginate and Suwannee River humic acids. pH and
42 concentration effects on nanoparticle stability. *Water Research* **2013**, *47* (16), 6052-6063.

43
44 22. Louie, S. M.; Spielman-Sun, E. R.; Small, M. J.; Tilton, R. D.; Lowry, G. V.,
45 Correlation of the Physicochemical Properties of Natural Organic Matter Samples from
46
47
48
49
50
51
52
53
54
55
56
57
58
59
60

1
2
3 Different Sources to Their Effects on Gold Nanoparticle Aggregation in Monovalent
4 Electrolyte. *Environmental Science & Technology* **2015**, *49* (4), 2188-2198.

5
6 23. Louie, S. M.; Tilton, R. D.; Lowry, G. V., Effects of Molecular Weight
7 Distribution and Chemical Properties of Natural Organic Matter on Gold Nanoparticle
8 Aggregation. *Environmental Science & Technology* **2013**, *47* (9), 4245-4254.

9
10 24. Nason, J. A.; McDowell, S. A.; Callahan, T. W., Effects of natural organic matter
11 type and concentration on the aggregation of citrate-stabilized gold nanoparticles. *Journal*
12 *of Environmental Monitoring* **2012**, *14* (7), 1885-1892.

13
14 25. Shen, M. H.; Yin, Y. G.; Booth, A.; Liu, J. F., Effects of molecular weight-
15 dependent physicochemical heterogeneity of natural organic matter on the aggregation of
16 fullerene nanoparticles in mono- and di-valent electrolyte solutions. *Water Res* **2015**, *71*,
17 11-20.

18
19 26. Deonarine, A.; Lau, B. L. T.; Aiken, G. R.; Ryan, J. N.; Hsu-Kim, H., Effects
20 of Humic Substances on Precipitation and Aggregation of Zinc Sulfide Nanoparticles.
21 *Environmental Science & Technology* **2011**, *45* (8), 3217-3223.

22
23 27. D'Andrilli, J.; Dittmar, T.; Koch, B. P.; Purcell, J. M.; Marshall, A. G.; Cooper,
24 W. T., Comprehensive characterization of marine dissolved organic matter by Fourier
25 transform ion cyclotron resonance mass spectrometry with electrospray and atmospheric
26 pressure photoionization. *Rapid Communications in Mass Spectrometry* **2010**, *24* (5),
27 643-650.

28
29 28. Sikder, M.; Wang, J.; Thomas Chandler, G.; Berti, D.; Baalousha, M., Synthesis,
30 Characterization, and Environmental Behaviors of Monodispersed Platinum
31 Nanoparticles. *Journal of Colloid and Interface Science* **2019**.

32
33 29. Filipe, V.; Hawe, A.; Jiskoot, W., Critical Evaluation of Nanoparticle Tracking
34 Analysis (NTA) by NanoSight for the Measurement of Nanoparticles and Protein
35 Aggregates. *Pharmaceutical Research* **2010**, *27* (5), 796-810.

36
37 30. Gottschalk, F.; Sonderer, T.; Scholz, R. W.; Nowack, B., Modeled
38 Environmental Concentrations of Engineered Nanomaterials (TiO₂, ZnO, Ag, CNT,
39 Fullerenes) for Different Regions. *Environmental Science & Technology* **2009**, *43* (24),
40 9216-9222.

41
42 31. Loosli, F.; Wang, J.; Rothenberg, S.; Bizimis, M.; Winkler, C.; Borovinskaya,
43 O.; Flamigni, L.; Baalousha, M., Sewage spills are a major source of titanium dioxide
44
45
46
47
48
49
50
51
52
53
54
55
56
57
58
59
60

1
2
3 engineered (nano)-particle release into the environment. *Environmental Science: Nano*
4 **2019**.

5
6 32. Baalousha, M.; Sikder, M.; Prasad, A.; Lead, J.; Merrifield, R.; Chandler, G.
7 T., The concentration-dependent behaviour of nanoparticles. *Environmental Chemistry*
8 **2016**, *13* (1), 1-3.

9
10 33. Bocca, B.; Petrucci, F.; Alimonti, A.; Caroli, S., Traffic-related platinum and
11 rhodium concentrations in the atmosphere of Rome. *Journal of Environmental*
12 *Monitoring* **2003**, *5* (4), 563-568.

13
14 34. Schäfer, J.; Puchelt, H., Platinum-Group-Metals (PGM) emitted from automobile
15 catalytic converters and their distribution in roadside soils. *Journal of Geochemical*
16 *Exploration* **1998**, *64* (1), 307-314.

17
18 35. Morton, O.; Puchelt, H.; Hernández, E.; Lounejeva, E., Traffic-related platinum
19 group elements (PGE) in soils from Mexico City. *Journal of Geochemical Exploration*
20 **2001**, *72* (3), 223-227.

21
22 36. Artelt, S.; Creutzenberg, O.; Kock, H.; Levsen, K.; Nachtigall, D.; Heinrich,
23 U.; Rühle, T.; Schlögl, R., Bioavailability of fine dispersed platinum as emitted from
24 automotive catalytic converters: a model study. *Science of The Total Environment* **1999**,
25 *228* (2), 219-242.

26
27 37. Barbante, C.; Veysseyre, A.; Ferrari, C.; Van De Velde, K.; Morel, C.;
28 Capodaglio, G.; Cescon, P.; Scarponi, G.; Boutron, C., Greenland Snow Evidence of
29 Large Scale Atmospheric Contamination for Platinum, Palladium, and Rhodium.
30 *Environmental Science & Technology* **2001**, *35* (5), 835-839.

31
32 38. Moldovan, M.; Rauch, S.; Gómez, M.; Antonia Palacios, M.; Morrison, G. M.,
33 Bioaccumulation of palladium, platinum and rhodium from urban particulates and
34 sediments by the freshwater isopod *Asellus aquaticus*. *Water Research* **2001**, *35* (17),
35 4175-4183.

36
37 39. Folens, K.; Van Acker, T.; Bolea-Fernandez, E.; Cornelis, G.; Vanhaecke, F.;
38 Du Laing, G.; Rauch, S., Identification of platinum nanoparticles in road dust leachate by
39 single particle inductively coupled plasma-mass spectrometry. *Science of The Total*
40 *Environment* **2018**, *615*, 849-856.

41
42 40. Ravindra, K.; Bencs, L.; Van Grieken, R., Platinum group elements in the
43 environment and their health risk. *Science of The Total Environment* **2004**, *318* (1), 1-43.
44
45
46
47
48
49
50
51
52
53
54
55
56
57
58
59
60

- 1
2
3 41. Pawlak, J.; Łodyga-Chruścińska, E.; Chrustowicz, J., Fate of platinum metals in
4 the environment. *Journal of Trace Elements in Medicine and Biology* **2014**, *28* (3), 247-
5 254.
6
7
8 42. Biesinger, K. E.; Christensen, G. M., Effects of Various Metals on Survival,
9 Growth, Reproduction, and Metabolism of *Daphnia magna*. *Journal of the Fisheries*
10 *Research Board of Canada* **1972**, *29* (12), 1691-1700.
11
12 43. Veltz, I.; Arsac, F.; Biagianti-Risbourg, S.; Habets, F.; Lechenault, H.; Vernet,
13 G., Effects of platinum (Pt⁴⁺) on *Lumbriculus variegatus* Muller (Annelida,
14 Oligochaetae): acute toxicity and bioaccumulation. *Arch Environ Contam Toxicol* **1996**,
15 *31* (1), 63-7.
16
17 44. Książyk, M.; Asztemborska, M.; Stęborowski, R.; Bystrzejewska-Piotrowska,
18 G., Toxic Effect of Silver and Platinum Nanoparticles Toward the Freshwater Microalga
19 *Pseudokirchneriella subcapitata*. *Bulletin of Environmental Contamination and*
20 *Toxicology* **2015**, *94* (5), 554-558.
21
22 45. Wei, C.; Morrison, G. M., Platinum in Road Dusts and Urban River Sediments.
23 *Science of the Total Environment* **1994**, *146*, 169-174.
24
25 46. Koczur, K. M.; Mourdikoudis, S.; Polavarapu, L.; Skrabalak, S. E.,
26 Polyvinylpyrrolidone (PVP) in nanoparticle synthesis. *Dalton Transactions* **2015**, *44*
27 (41), 17883-17905.
28
29 47. Gatan Incorporation. In *Gatan Digital Micrograph Software Instalation*
30 *Instructions*, 2018.
31
32 48. Aiken, G. R.; McKnight, D. M.; Thorn, K. A.; Thurman, E. M., Isolation of
33 hydrophilic organic acids from water using nonionic macroporous resins. *Organic*
34 *Geochemistry* **1992**, *18* (4), 567-573.
35
36 49. Graham, A. M.; Aiken, G. R.; Gilmour, C. C., Effect of Dissolved Organic Matter
37 Source and Character on Microbial Hg Methylation in Hg-S-DOM Solutions.
38 *Environmental Science & Technology* **2013**, *47* (11), 5746-5754.
39
40 50. Jiang, C.; Castellon, B. T.; Matson, C. W.; Aiken, G. R.; Hsu-Kim, H., Relative
41 Contributions of Copper Oxide Nanoparticles and Dissolved Copper to Cu Uptake
42 Kinetics of Gulf Killifish (*Fundulus grandis*) Embryos. *Environmental Science &*
43 *Technology* **2017**, *51* (3), 1395-1404.
44
45 51. Poulin, B. A.; Ryan, J. N.; Nagy, K. L.; Stubbins, A.; Dittmar, T.; Orem, W.;
46 Krabbenhoft, D. P.; Aiken, G. R., Spatial Dependence of Reduced Sulfur in Everglades
47
48
49
50
51
52
53
54
55
56
57
58
59
60

1
2
3 Dissolved Organic Matter Controlled by Sulfate Enrichment. *Environmental Science &*
4 *Technology* **2017**, *51* (7), 3630-3639.

5
6 52. Green, N. W.; Perdue, E. M.; Aiken, G. R.; Butler, K. D.; Chen, H.; Dittmar,
7 T.; Niggemann, J.; Stubbins, A., An intercomparison of three methods for the large-scale
8 isolation of oceanic dissolved organic matter. *Marine Chemistry* **2014**, *161*, 14-19.

9
10 53. Huffman, E. W. D.; Stuber, H. A., Analytical methodology for elemental analysis
11 of humic substances. In *Humic Substances in Soil, Sediment, and Water: Geochemistry,*
12 *Isolation, and Characterization*, Wiley: 1985; pp 433-456.

13
14 54. Weishaar, J. L.; Aiken, G. R.; Bergamaschi, B. A.; Fram, M. S.; Fujii, R.;
15 Mopper, K., Evaluation of Specific Ultraviolet Absorbance as an Indicator of the
16 Chemical Composition and Reactivity of Dissolved Organic Carbon. *Environmental*
17 *Science & Technology* **2003**, *37* (20), 4702-4708.

18
19 55. Tolić, N.; Liu, Y.; Liyu, A.; Shen, Y.; Tfaily, M. M.; Kujawinski, E. B.;
20 Longnecker, K.; Kuo, L.-J.; Robinson, E. W.; Paša-Tolić, L.; Hess, N. J., Formularity:
21 Software for Automated Formula Assignment of Natural and Other Organic Matter from
22 Ultrahigh-Resolution Mass Spectra. *Analytical Chemistry* **2017**, *89* (23), 12659-12665.

23
24 56. Tfaily, M. M.; Chu, R. K.; Tolić, N.; Roscioli, K. M.; Anderton, C. R.; Paša-
25 Tolić, L.; Robinson, E. W.; Hess, N. J., Advanced Solvent Based Methods for Molecular
26 Characterization of Soil Organic Matter by High-Resolution Mass Spectrometry.
27 *Analytical Chemistry* **2015**, *87* (10), 5206-5215.

28
29 57. Perminova, I. V.; Dubinenkov, I. V.; Kononikhin, A. S.; Konstantinov, A. I.;
30 Zhrebker, A. Y.; Andzhushev, M. A.; Lebedev, V. A.; Bulygina, E.; Holmes, R. M.;
31 Kostyukevich, Y. I.; Popov, I. A.; Nikolaev, E. N., Molecular Mapping of Sorbent
32 Selectivities with Respect to Isolation of Arctic Dissolved Organic Matter as Measured
33 by Fourier Transform Mass Spectrometry. *Environmental Science & Technology* **2014**,
34 *48* (13), 7461-7468.

35
36 58. Lee, S.; Bi, X.; Reed, R. B.; Ranville, J. F.; Herckes, P.; Westerhoff, P.,
37 Nanoparticle Size Detection Limits by Single Particle ICP-MS for 40 Elements.
38 *Environmental Science & Technology* **2014**, *48* (17), 10291-10300.

39
40 59. Ploc, R. A., Transmission electron microscopy of thin (<2000 Å) thermally formed
41 ZrO₂ films. *Journal of Nuclear Materials* **1968**, *28* (1), 48-60.

- 1
2
3 60. Tejamaya, M.; Romer, I.; Merrifield, R. C.; Lead, J. R., Stability of Citrate, PVP,
4 and PEG Coated Silver Nanoparticles in Ecotoxicology Media. *Environmental Science*
5 & *Technology* **2012**, *46* (13), 7011-7017.
6
7
8 61. El Badawy, A. M.; Scheckel, K. G.; Suidan, M.; Tolaymat, T., The impact of
9 stabilization mechanism on the aggregation kinetics of silver nanoparticles. *Sci Total*
10 *Environ* **2012**, *429*, 325-31.
11
12 62. Zhang, H.; Smith, J. A.; Oyanedel-Craver, V., The effect of natural water
13 conditions on the anti-bacterial performance and stability of silver nanoparticles capped
14 with different polymers. *Water Research* **2012**, *46* (3), 691-699.
15
16 63. Huynh, K. A.; Chen, K. L., Aggregation Kinetics of Citrate and
17 Polyvinylpyrrolidone Coated Silver Nanoparticles in Monovalent and Divalent
18 Electrolyte Solutions. *Environmental Science & Technology* **2011**, *45* (13), 5564-5571.
19
20 64. Lin, S.; Cheng, Y.; Liu, J.; Wiesner, M. R., Polymeric Coatings on Silver
21 Nanoparticles Hinder Autoaggregation but Enhance Attachment to Uncoated Surfaces.
22 *Langmuir* **2012**, *28* (9), 4178-4186.
23
24 65. Alexander, C. M.; Dabrowiak, J. C.; Goodisman, J., Gravitational sedimentation
25 of gold nanoparticles. *Journal of Colloid and Interface Science* **2013**, *396*, 53-62.
26
27 66. Pettibone, J. M.; Cwiertny, D. M.; Scherer, M.; Grassian, V. H., Adsorption of
28 Organic Acids on TiO₂ Nanoparticles: Effects of pH, Nanoparticle Size, and
29 Nanoparticle Aggregation. *Langmuir* **2008**, *24* (13), 6659-6667.
30
31 67. Stankus, D. P.; Lohse, S. E.; Hutchison, J. E.; Nason, J. A., Interactions between
32 Natural Organic Matter and Gold Nanoparticles Stabilized with Different Organic
33 Capping Agents. *Environmental Science & Technology* **2011**, *45* (8), 3238-3244.
34
35 68. Zhang, H.; Penn, R. L.; Hamers, R. J.; Banfield, J. F., Enhanced Adsorption of
36 Molecules on Surfaces of Nanocrystalline Particles. *The Journal of Physical Chemistry*
37 *B* **1999**, *103* (22), 4656-4662.
38
39 69. Chin, Y.-P.; Aiken, G.; O'Loughlin, E., Molecular Weight, Polydispersity, and
40 Spectroscopic Properties of Aquatic Humic Substances. *Environmental Science &*
41 *Technology* **1994**, *28* (11), 1853-1858.
42
43 70. Phenrat, T.; Song, J. E.; Cisneros, C. M.; Schoenfelder, D. P.; Tilton, R. D.;
44 Lowry, G. V., Estimating Attachment of Nano- and Submicrometer-particles Coated with
45 Organic Macromolecules in Porous Media: Development of an Empirical Model.
46 *Environmental Science & Technology* **2010**, *44* (12), 4531-4538.
47
48
49
50
51
52
53
54
55
56
57
58
59
60

- 1
2
3 71. Tiller, C. L.; O'Melia, C. R., Natural organic matter and colloidal stability: Models
4 and measurements. *Colloids and Surfaces A: Physicochemical and Engineering Aspects*
5 **1993**, *73*, 89-102.
6
7
8 72. Au, K.-K.; Penisson, A. C.; Yang, S.; O'Melia, C. R., Natural organic matter at
9 oxide/water interfaces: complexation and conformation. *Geochimica et Cosmochimica*
10 *Acta* **1999**, *63* (19), 2903-2917.
11
12 73. Baalousha, M.; Afshinnia, K.; Guo, L., Natural organic matter composition
13 determines the molecular nature of silver nanomaterial-NOM corona. *Environmental*
14 *Science: Nano* **2018**, *5* (4), 868-881.
15
16 74. Avneri-Katz, S.; Young, R. B.; McKenna, A. M.; Chen, H.; Corilo, Y. E.;
17 Polubesova, T.; Borch, T.; Chefetz, B., Adsorptive fractionation of dissolved organic
18 matter (DOM) by mineral soil: Macroscale approach and molecular insight. *Organic*
19 *Geochemistry* **2017**, *103*, 113-124.
20
21 75. Davis, J. A.; Gloor, R., Adsorption of dissolved organics in lake water by
22 aluminum oxide. Effect of molecular weight. *Environmental Science & Technology* **1981**,
23 *15* (10), 1223-1229.
24
25 76. Lv, J.; Zhang, S.; Wang, S.; Luo, L.; Cao, D.; Christie, P., Molecular-Scale
26 Investigation with ESI-FT-ICR-MS on Fractionation of Dissolved Organic Matter
27 Induced by Adsorption on Iron Oxyhydroxides. *Environmental Science & Technology*
28 **2016**, *50* (5), 2328-2336.
29
30 77. Mwaanga, P.; Carraway, E. R.; Schlautman, M. A., Preferential sorption of some
31 natural organic matter fractions to titanium dioxide nanoparticles: influence of pH and
32 ionic strength. *Environ Monit Assess* **2014**, *186* (12), 8833-44.
33
34 78. Zhou, Q.; Maurice, P. A.; Cabaniss, S. E., Size fractionation upon adsorption of
35 fulvic acid on goethite: equilibrium and kinetic studies. *Geochimica et Cosmochimica*
36 *Acta* **2001**, *65* (5), 803-812.
37
38 79. Haslam, E., *Practical polyphenolics: from structure to molecular recognition and*
39 *physiological action*. Cambridge University Press: Cambridge, 1998.
40
41 80. Sipponen, M. H.; Lange, H.; Ago, M.; Crestini, C., Understanding Lignin
42 Aggregation Processes. A Case Study: Budesonide Entrapment and Stimuli Controlled
43 Release from Lignin Nanoparticles. *ACS Sustainable Chemistry & Engineering* **2018**, *6*
44 (7), 9342-9351.
45
46
47
48
49
50
51
52
53
54
55
56
57
58
59
60

- 1
2
3 81. Lal, R., Mechanisms of Carbon Sequestration in Soil Aggregates AU - Blanco-
4 Canqui, Humberto. *Critical Reviews in Plant Sciences* **2004**, 23 (6), 481-504.
5
6 82. Caesar-TonThat, T. C.; Cochran, V. L., Soil aggregate stabilization by a
7 saprophytic lignin-decomposing basidiomycete fungus I. Microbiological aspects.
8 *Biology and Fertility of Soils* **2000**, 32 (5), 374-380.
9
10 83. Xiao, C.; Bolton, R.; Pan, W. L., Lignin from rice straw Kraft pulping: Effects
11 on soil aggregation and chemical properties. *Bioresource Technology* **2007**, 98 (7), 1482-
12 1488.
13
14
15
16
17
18
19
20
21
22
23
24
25
26
27
28
29
30
31
32
33
34
35
36
37
38
39
40
41
42
43
44
45
46
47
48
49
50
51
52
53
54
55
56
57
58
59
60

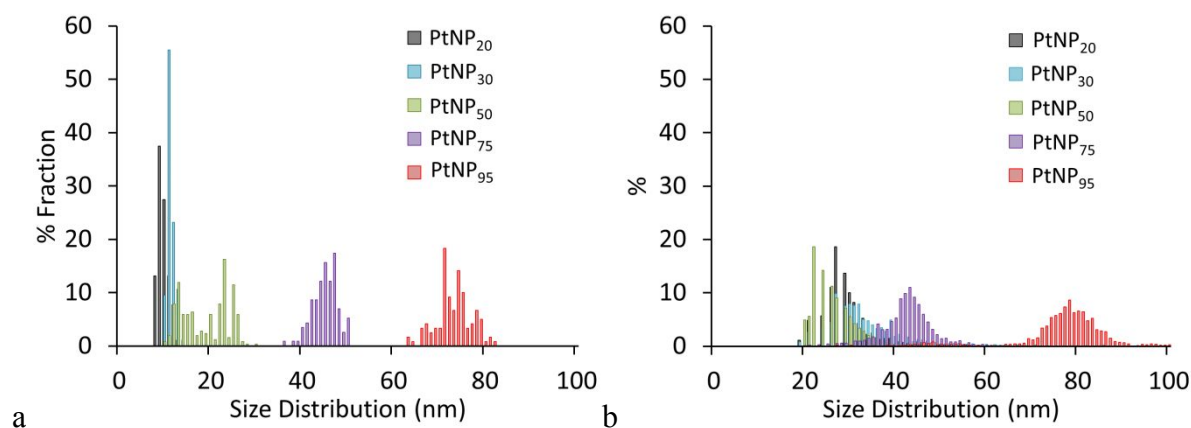


Figure 1. Number particle size distribution of polyvinylpyrrolidone-coated platinum nanoparticles of five different nominal sizes ranging from 20 to 95 nm (denoted as PtNP₂₀-PtNP₉₅) measured by (a) transmission electron microscope (TEM), and (b) single particle-inductively coupled plasma-mass spectrometer (sp-ICP-MS). Size detection limit of PtNPs in sp-ICP-MS is 18 nm.

Sample ID	in UPW- 0 h		in MHW- 0 h		in MHW- 24 h	
	Pt conc. ($\mu\text{g L}^{-1}$)	% measured relative to the nominal conc.	Pt conc. ($\mu\text{g L}^{-1}$)	% measured relative to the nominal conc.	Pt conc. ($\mu\text{g L}^{-1}$)	% measured relative to the nominal conc.
PtNP ₂₀	0.017 ± 0.007	1.7 ± 0.7	0.209 ± 0.004	20.9 ± 0.4	0.583 ± 0.016	58.3 ± 1.6
PtNP ₃₀	0.082 ± 0.007	8.2 ± 0.7	0.426 ± 0.057	42.6 ± 5.7	0.583 ± 0.015	58.3 ± 1.5
PtNP ₅₀	0.313 ± 0.036	31.3 ± 3.6	0.290 ± 0.048	29.0 ± 4.8	0.046 ± 0.012	4.60 ± 1.2
PtNP ₇₅	0.851 ± 0.029	85.1 ± 2.9	0.813 ± 0.048	81.3 ± 4.8	0.685 ± 0.049	68.5 ± 4.9
PtNP ₉₅	0.824 ± 0.028	82.4 ± 2.8	0.706 ± 0.015	70.6 ± 1.5	0.373 ± 0.003	37.3 ± 0.3

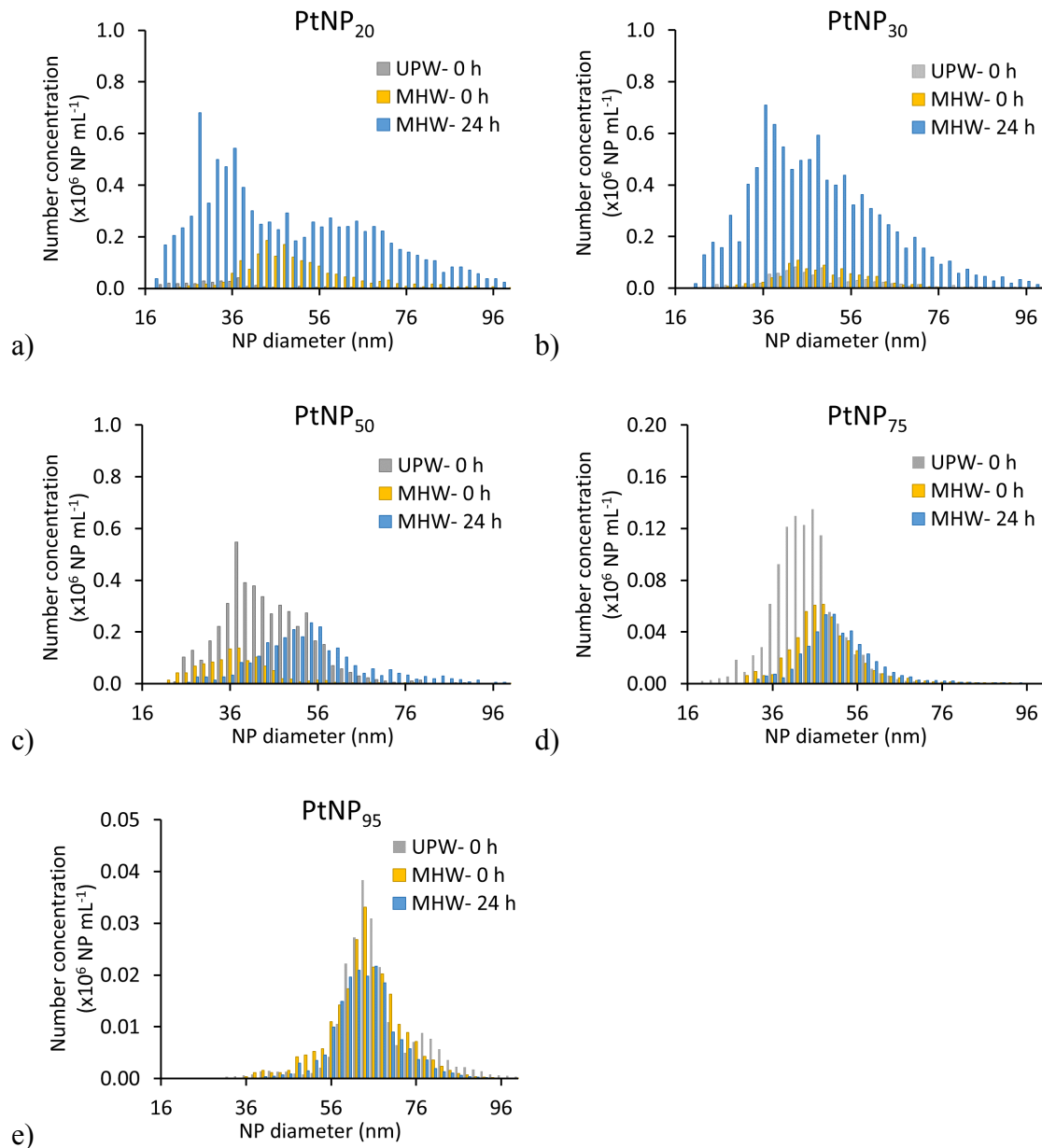


Figure 2. Number particle size distribution (PSDs) measured by sp-ICP-MS of 1 $\mu\text{g L}^{-1}$ PVP-PtNPs in ultrapure water (UPW) at 0 and 24 h after mixing with moderately hard water (MHW) of: (a) PtNP₂₀, (b) PtNP₃₀, (c) PtNP₅₀, (d) PtNP₇₅, and (e) PtNP₉₅.

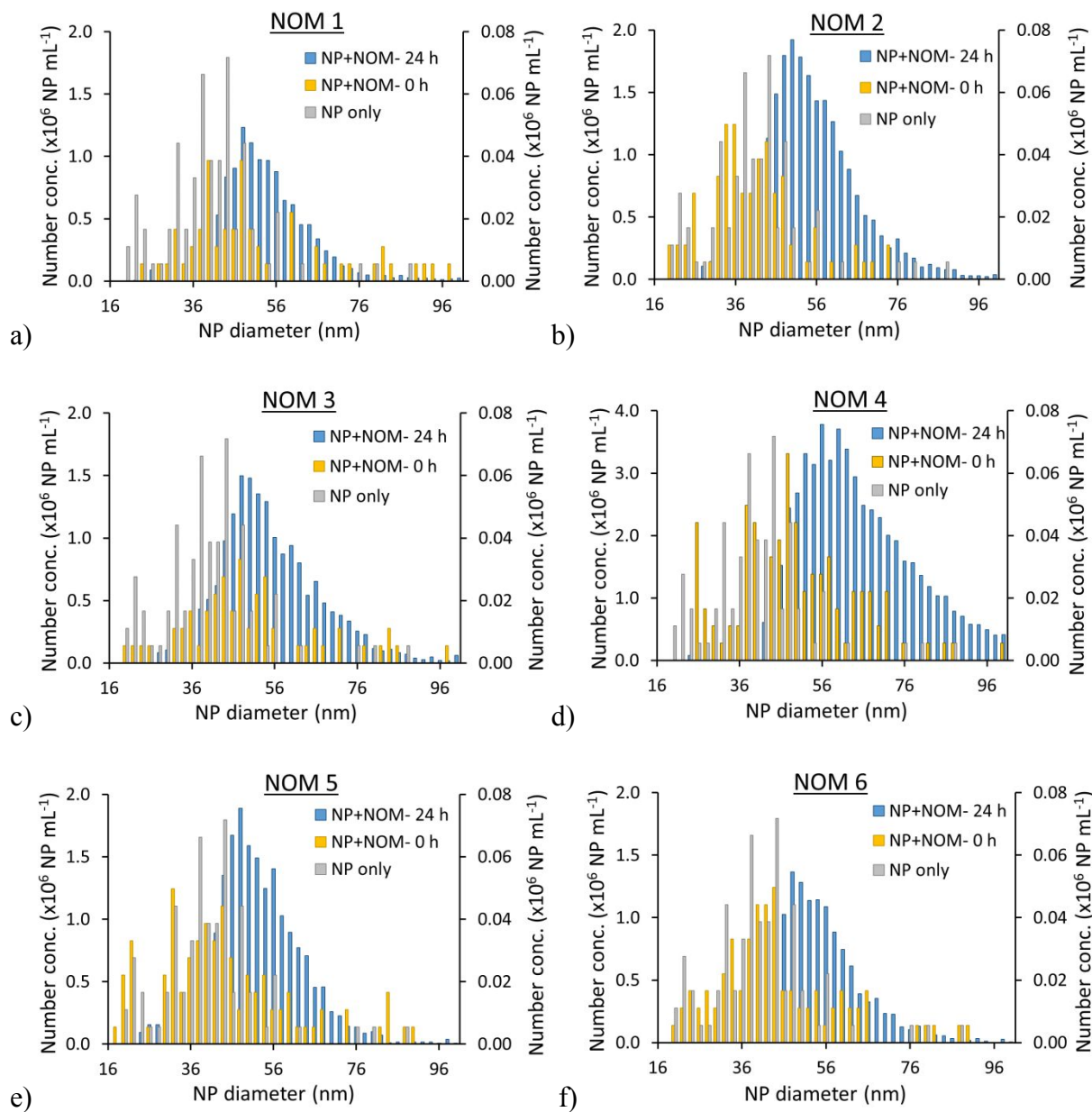


Figure 3. Particle size distribution (PSD) measured by sp-ICP-MS of $1 \mu\text{g L}^{-1}$ PtNP₂₀ at 0 and 24 hours after mixing with MHW in presence of 1mg L^{-1} (a) NOM 1, (b) NOM 2, (c) NOM 3, (d) NOM 4, (e) NOM 5, and (f) NOM 6. The number concentration of PtNPs only and PtNPs+NOM- at 0 h are presented on the secondary Y-axis.

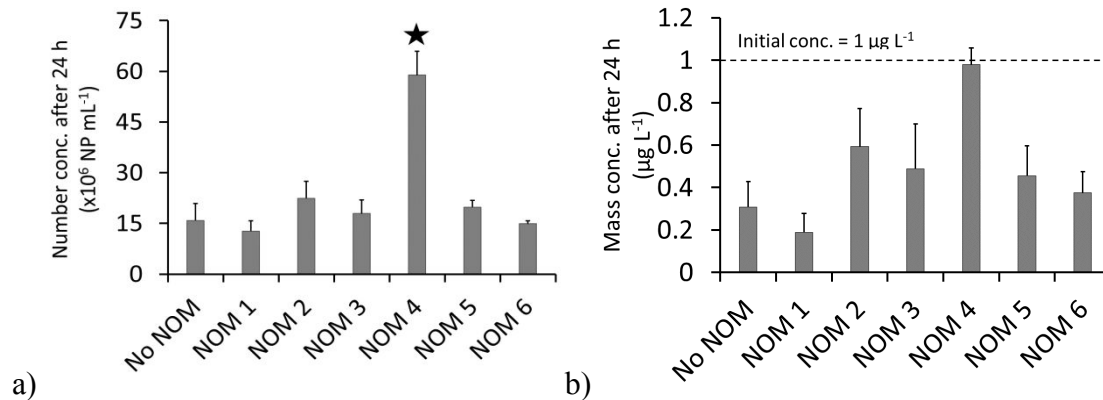


Figure 4. (a) Number and (b) mass concentration of 1 µg L⁻¹ PtNP₂₀ measured by sp-ICP-MS after 24 h of mixing with MHW in absence and presence of 1 mg L⁻¹ NOM. * represents a significant increase in measured PtNP₂₀ number concentration in presence of NOM compared to that measured in the absence of NOM.

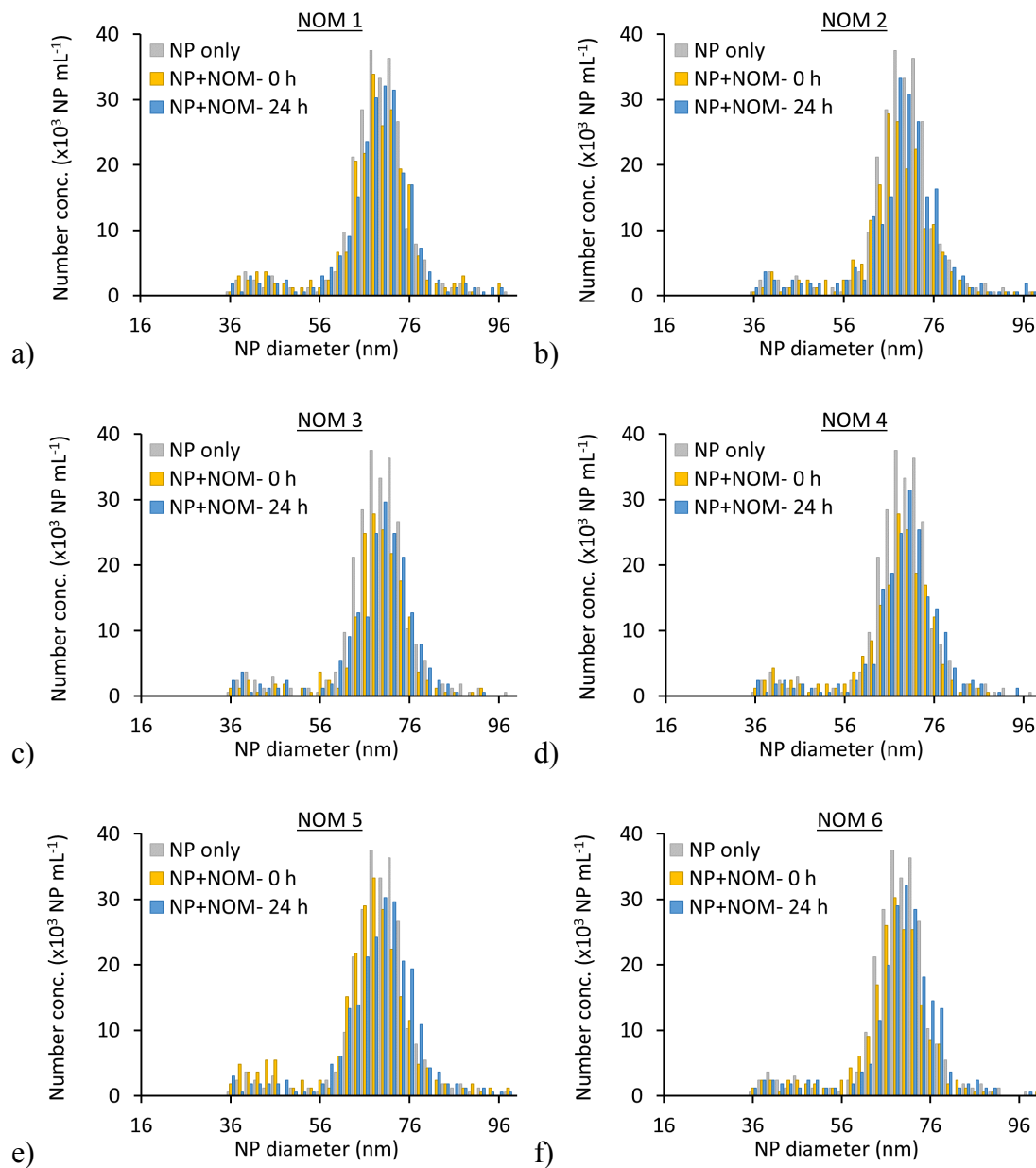


Figure 5. Particle size distribution of PtNP₉₅ measured by sp-ICP-MS of 1 µg L⁻¹ PtNP₉₅ at 0 h and 24 h after mixing with MHW in presence of 1 mg L⁻¹ (a) NOM 1, (b) NOM 2, (c) NOM 3, (d) NOM 4, (e) NOM 5, and (f) NOM 6.

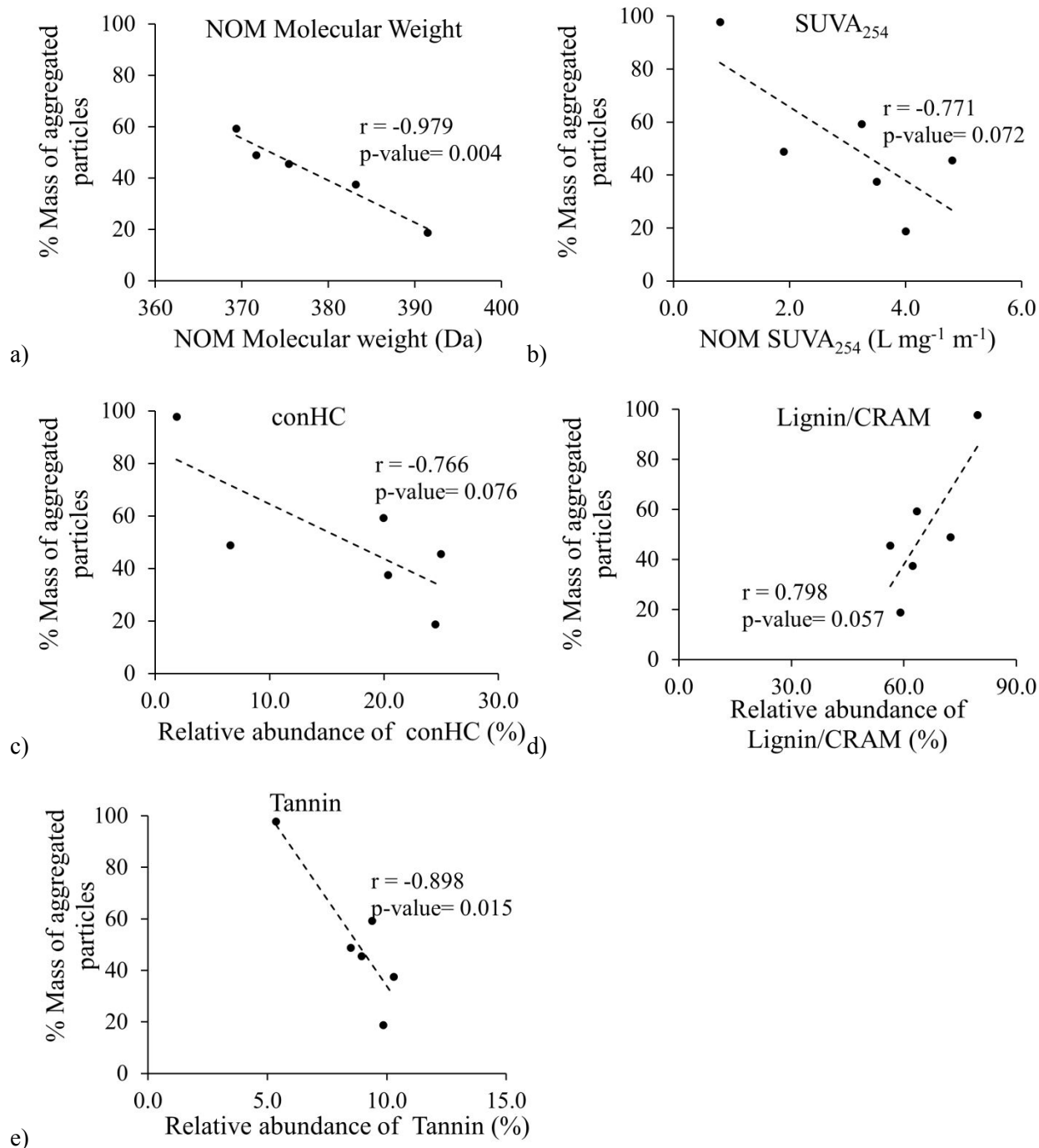


Figure 6. Correlation between % of PtNP₂₀ mass undergoing aggregation in presence of the different NOM isolates and NOM properties: (a) molecular weight, (b) specific UV absorbance at 254 nm (SUVA₂₅₄), (c) condensed hydrocarbon (ConHC), (d) lignin/carboxyl-rich alicyclic molecules (CRAM), and (e) tannin. The Pearson's correlation coefficient (r) and p-values of linear regressions are presented for each plot.

Table 1. Analysis results of Pearson's correlation between aggregated PtNP₂₀ mass and NOM properties. * indicates correlations with statistical significance

Variables	Pearson's correlation coefficient (r)	p-value
% mass of aggregated NP vs NOM elemental composition		
O	-0.411	0.418
N	-0.164	0.756
S	-0.429	0.397
SUVA ₂₅₄	-0.771	0.072
Molecular weight	-0.979	0.004*
O/C	-0.841	0.036*
H/C	0.730	0.099
% mass of aggregated NP vs NOM formula assignments by compound classes		
Aminosugar	0.709	0.115
Condensed HC	-0.766	0.076
Carbohydrates	-0.746	0.089
Lignin	0.798	0.058
Lipid	0.409	0.420
Protein	0.748	0.087
Tannin	-0.898	0.015*
Unsaturated HC	-0.171	0.745